Electronic Supplementary Material (ESI) for Dalton Transactions.
This journal is © The Royal Society of Chemistry 2023

*Supporting Information for*

# Enhancing the Electrocatalytic Activities of Metal Organic Frameworks for Oxygen Evolution Reaction with Bimetallic Groups

Yumeng Li[a], Belvin Thomas[b], Chaoyun Tang[a,b,#] and Tewodros Asefa[a,b,*]

[a] Department of Chemical and Biochemical Engineering, Rutgers, The State University of New Jersey, 98 Brett Road, Piscataway, NJ 08854, USA

[b] Department of Chemistry and Chemical Biology, Rutgers, The State University of New Jersey, 610 Taylor Road, Piscataway, NJ 08854, USA

[#] Current address: Department of Chemical Engineering, University of Massachusetts at Amherst, 210A Goessmann Laboratory, 686 North Pleasant St., Amherst, MA 01003, USA

* Corresponding author's e-mail: tasefa@chem.rutgers.edu

## 1. Additional Results and Discussions on $Co_xNi_y$-MOF Materials or Electrocatalysts

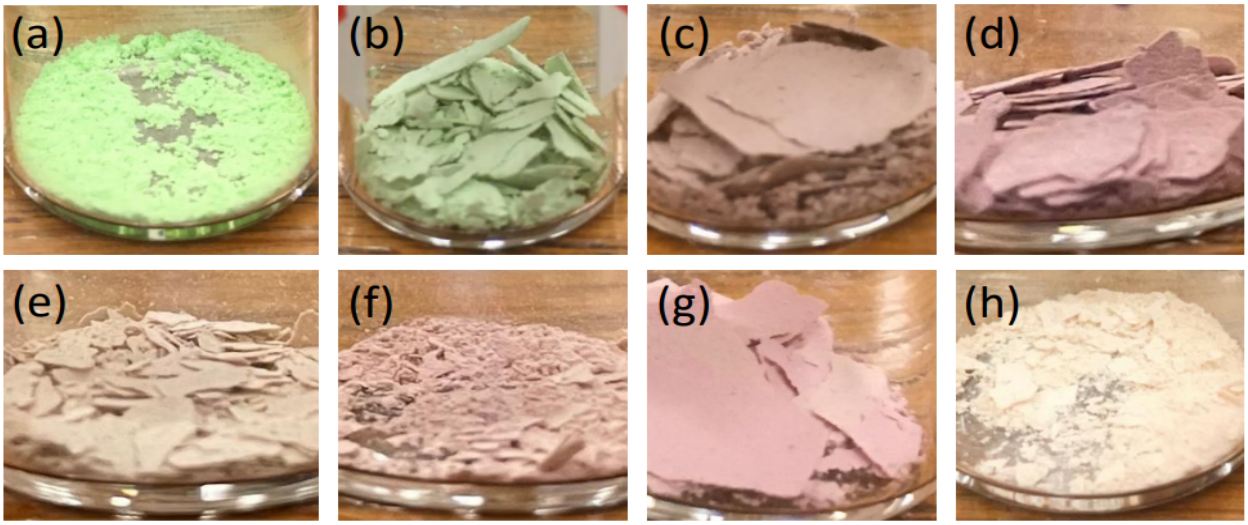


**Figure S1.** The physical appearance of as-synthesized monometallic and bimetallic MOFs: (a) Ni-MOF, (b) $Co_1Ni_{20}$-MOF, (c) $Co_1Ni_1$-MOF, (d) $Co_5Ni_1$-MOF, (e) $Co_{10}Ni_1$-MOF, (f) $Co_{15}Ni_1$-MOF, (g) $Co_{20}Ni_1$-MOF, and (h) Co-MOF.

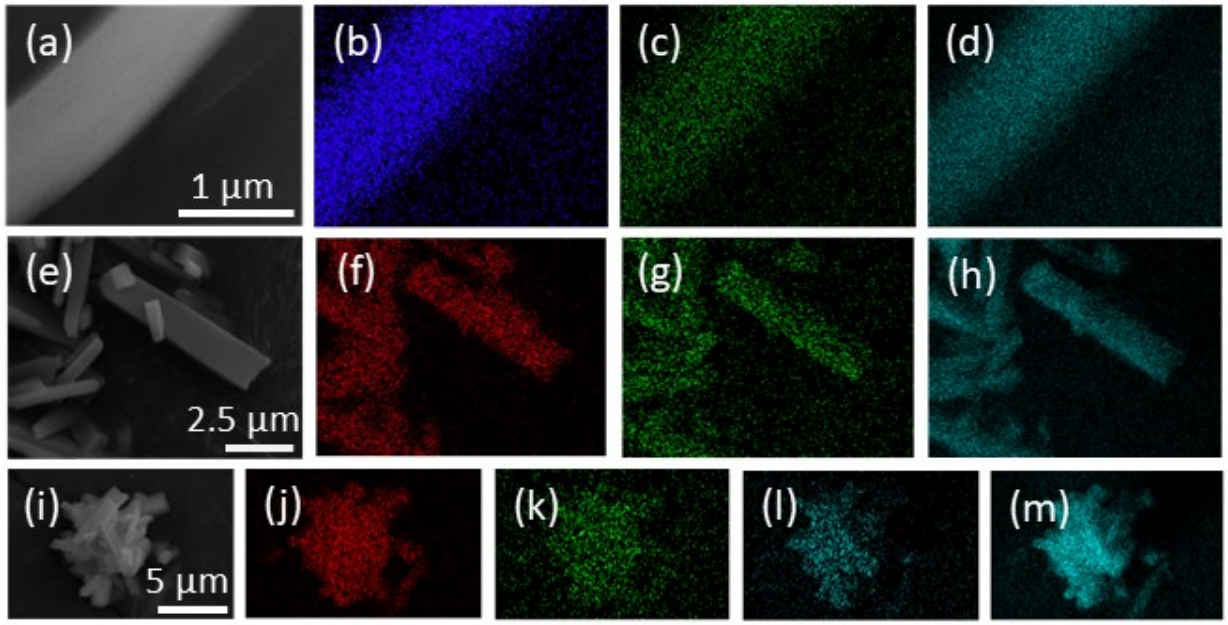


**Figure S2.** SEM and SEM-EDX elemental mapping images of different MOF materials. The images are for (a) SEM image of the portion of Co-MOF as analyzed by EDX showing the elements (b) Co, (c) N, and (d) O in it; (e) SEM image of the portion of Ni-MOF as analyzed by EDX showing the elements (f) Ni, (g) N, and (h) O in it; (i) SEM image of the portion of $Co_{10}Ni_1$-MOF as analyzed by EDX showing the elements (j) Co, (k) Ni, (l) N, and (m) O in it.

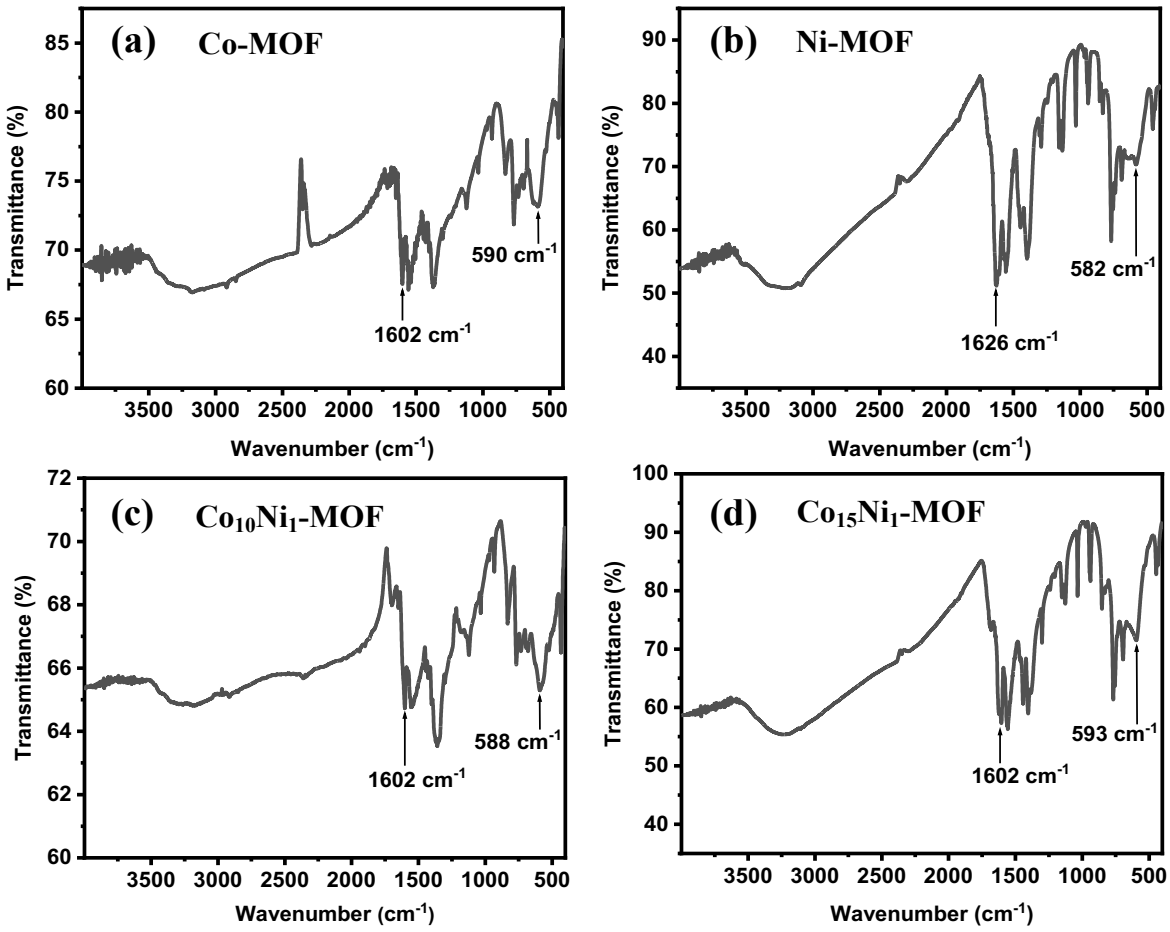


**Figure S3.** FT-IR spectra of (a) Co-MOF, (b) Ni-MOF, (c) $Co_{10}Ni_1$-MOF, and (d) $Co_{15}Ni_1$-MOF.

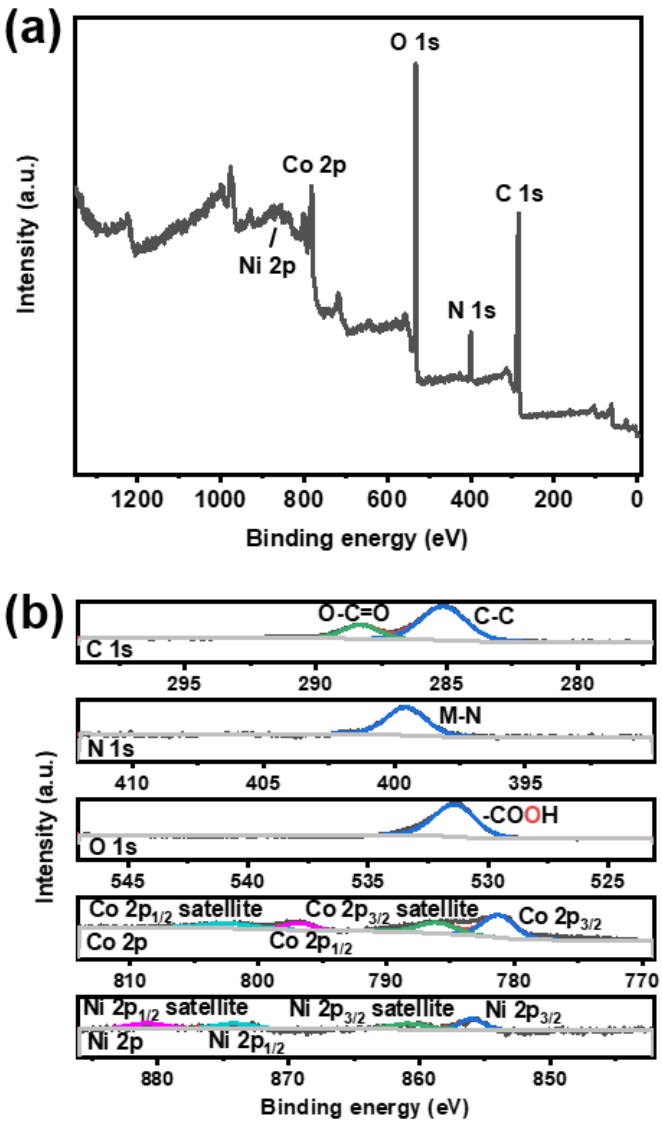


**Figure S4.** (a) Survey XPS spectrum of $Co_{10}Ni_1$-MOF. (b) High-resolution XPS spectra of peaks corresponding to C 1s, N 1s, O 1s, Co 2p, and Ni 2p of $Co_{10}Ni_1$-MOF.

## 2. Synthesis and Characterization of Mn-MOF and $Co_xMn_y$-MOFs

To demonstrate the versatility of the synthetic method to other related materials, a series of bimetallic Co- and Mn-based MOF materials and the corresponding monometallic MOFs (the reference materials) are synthesized using the same synthetic method, except by using Co(II) and Mn(II) ions. Furthermore, by varying the relative ratio of these two metal ions, here also, the compositions of the bimetallic Co-Mn-MOFs are varied. The physical appearance of the resulting MOF materials, named $Co_xMn_z$-MOFs, and the reference material Mn-MOFs are shown in Figure S5. Here too the colors of the materials slightly vary according to the metals they contain. The best performing electrocatalyst for OER from the resulting materials is found to be $Co_{10}Mn_1$-MOF

(see below). This material is further studied experimentally to determine if $Co^{3+}$ species that form on it during the activation of the material during OER is the electrocatalytic active site in it as well.

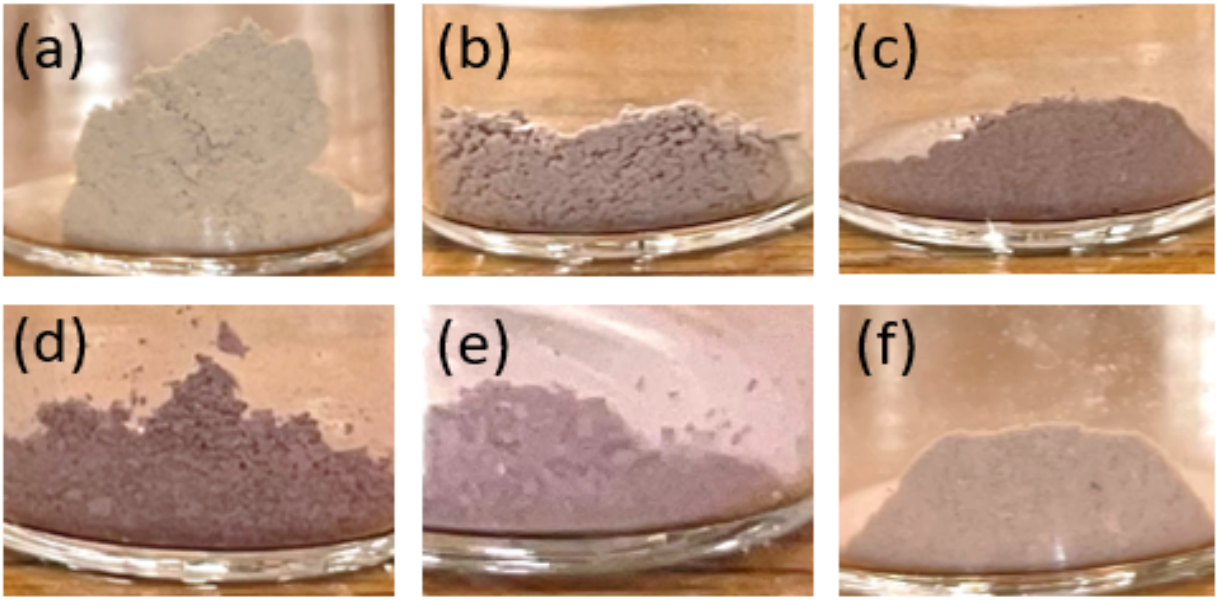


**Figure S5.** The appearance of (a) Mn-MOF, (b) $Co_1Mn_5$-MOF, (c) $Co_1Mn_1$-MOF, (d) $Co_5Mn_1$-MOF, (e) $Co_{10}Mn_1$-MOF, and (f) $Co_{15}Mn_1$-MOF materials.

The powder XRD patterns of Co-MOF, Mn-MOF, and $Co_{10}Mn_1$-MOF are also taken and compared with one another to determine their crystallinity and the similarity/difference in their crystallinity between the bimetallic Co-Mn-MOF with respect to the monometallic counterparts (Figure S6). The XRD patterns of $Co_{10}Mn_1$-MOF and Co-MOF show the characteristic Bragg peak of Co-MOF at 2θ of ~15°. Just like Co-MOF, both Mn-MOF and $Co_{10}Mn_1$-MOF appear to have high crystallinity.

$Co_{10}Mn_1$-MOF is further characterized by SEM and TEM to determine its morphology and structure. Co-MOF and Mn-MOF are also imaged for comparison. The SEM images of the materials (Figures S7a-c) reveal that they all have 1D rod-like microstructures. Like $Co_xNi_y$-MOF materials, the ones containing Mn (i.e., Mn-MOF and $Co_{10}Mn_1$-MOF) show nanorod structures. The presence of Co makes them thinner though. Like the SEM images, TEM images of the $Co_{10}Mn_1$-MOF, Co-MOF, and Mn-MOF (Figures S7d-f) show uniform, non-porous structures throughout. Their TEM images also show a decrease in the widths of the nanorods when Co is included in this bimetallic MOF.

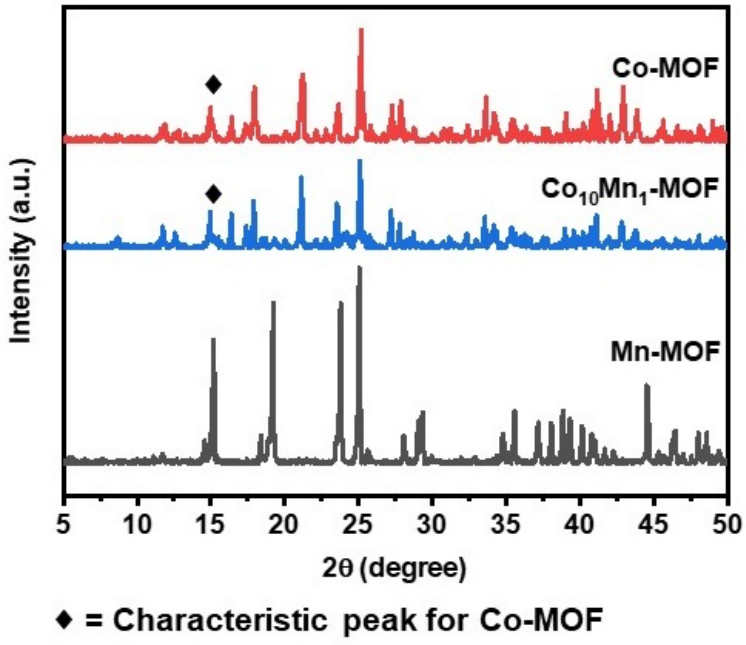


**Figure S6.** Powder XRD patterns of Co-MOF, $Co_{10}Mn_1$-MOF, and Mn-MOF materials.

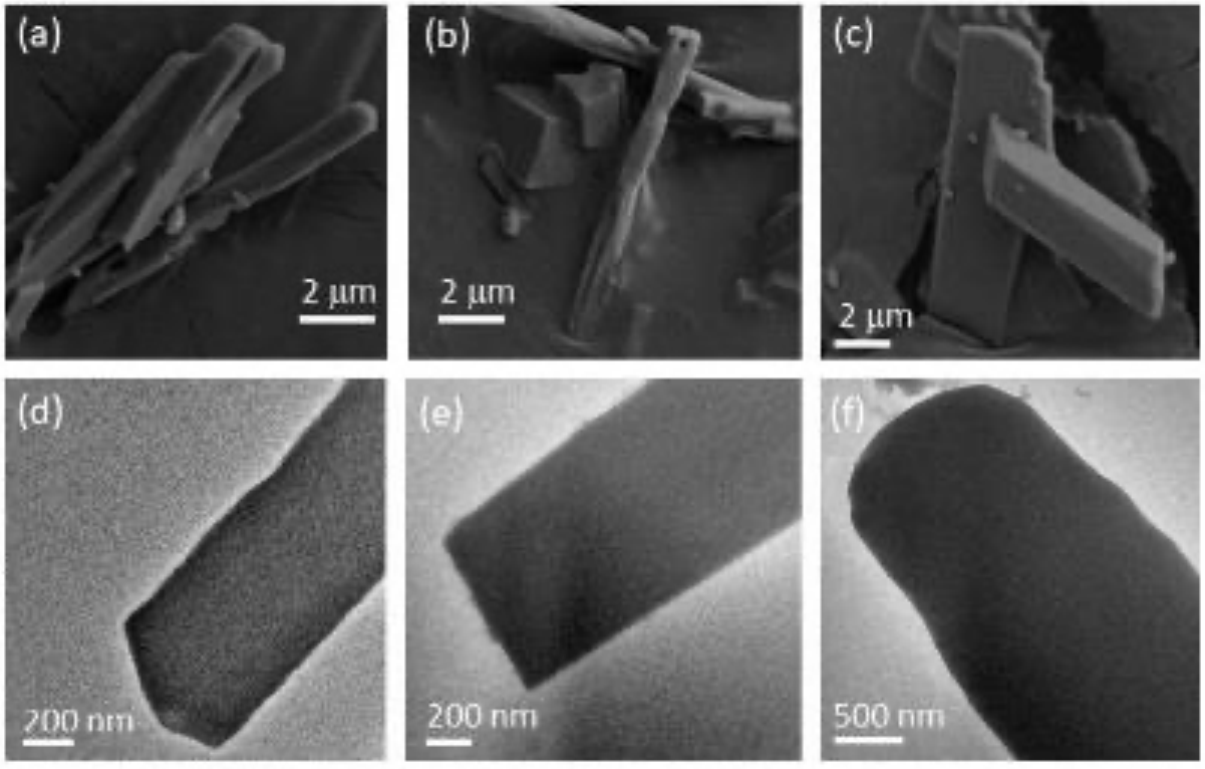


**Figure S7.** (a-c) SEM images Co-MOF, $Co_{10}Mn_1$-MOF, and Mn-MOF, respectively. (d-f) TEM images of Co-MOF, $Co_{10}Mn_1$-MOF, and Mn-MOF, respectively.

To evaluate the effect of the ratio of Co:Mn in the bimetallic MOFs on their electrocatalytic performances toward OER, linear sweep voltammetry curves are obtained for $Co_xMn_z$-MOFs composed of x:z = 15:1, 10:1, 5:1, 1:1, and 1:5 as well as for Co-MOF, Ni-MOF and Mn-MOF (i.e., the three reference monometallic MOF materials) (Figure S8). The results are compared with one another and also used to determine the degree of electrocatalytic activities of $Co_xMn_z$-MOF with respect to that of $Co_{15}Ni_1$-MOF (i.e., the best sample in the $Co_xNi_y$-MOF series). Based on the linear sweep voltammetry curves shown in Figure S8, the electrocatalytic performances of the bimetallic MOFs steadily increase until the ratio of x:z reaches 10:1. This result also indicate that Co and Mn in $Co_xMn_z$-MOFs exhibit a synergistic effect that enhances the OER performance, just like Co and Ni in $Co_xNi_y$-MOF did. However, the best electrocatalysts from the series of $Co_xMn_z$-MOF materials (i.e., $Co_{10}Mn_1$-MOF) performs lower than the $Co_{15}Ni_1$-MOF (the best one from the series of $Co_xNi_y$-MOF materials) in terms of both overpotential and maximum current density at 1.845 V vs. RHE.

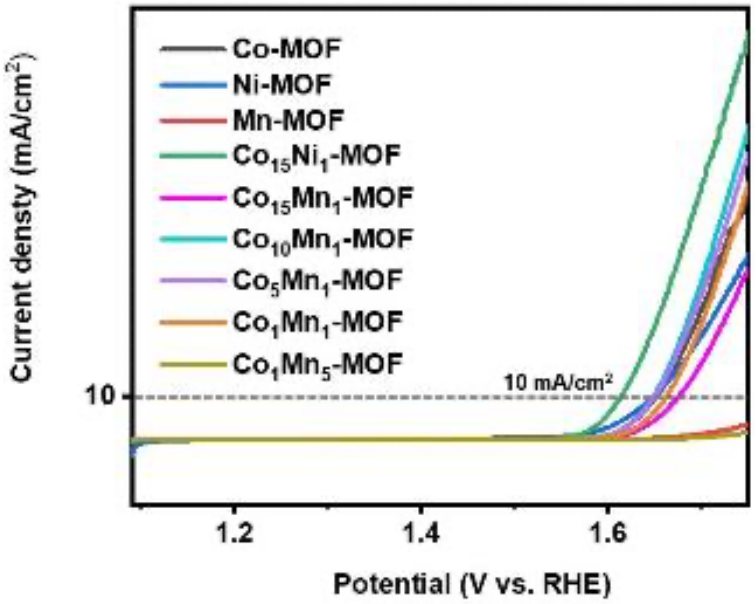


**Figure S8.** Comparison of the linear sweep voltammetry curves of OER as catalyzed by Co-MOF, Ni-MOF, Mn-MOF, $Co_{15}Ni_1$, and $Co_xMn_z$-MOF materials that are synthesized with x:z ratios of 15:1, 10:1, 5:1, 1:1, and 1:5 and with drying conditions of 60 ˚C for 24 h.

Further comparison of the changes in overpotential and maximum current density between the monometallic MOFs and bimetallic MOFs suggests that the synergistic effect manifested by the two metals differ depending on the combination of the metals involved. As shown in Table S1, the synergistic effect between Co and Ni in $Co_{15}Ni_1$-MOF is expressed by the large decrease in overpotential compared with the activity of Ni-MOF while the synergistic effect of Co and Mn in $Co_{10}Ni_1$-MOF is expressed by the rapid and large increase in maximum current density compared with the activity of Mn-MOF. These results suggest that an optimal combination of types of the two metals is important to obtain the bimetallic MOFs with low overpotential and increased maximum current density.

**Table S1.** Comparison of the changes in overpotential and maximum current density between the monometallic MOFs (Co-, Ni-, and Mn-MOF) and the bimetallic MOFs ($Co_{15}Ni_1$-MOF and $Co_{10}Mn_1$-MOF).

| **Materials** | **Change in overpotential at 10 mA/cm$^2$ (mV)** | **Change in maximum current density at 1.7 5 V vs. RHE (mA/cm$^2$)** |
|---|---|---|
| Ni-MOF to $Co_{15}Ni_1$-MOF | -186.5 | 49.6 |
| Co-MOF to $Co_{15}Ni_1$- MOF | -38.3 | 35.1 |
| Mn-MOF to $Co_{10}Mn_1$-MOF | -185.2 | 68.4 |
| Co-MOF to $Co_{10}Mn_1$-MOF | -30.7 | 14.6 |

Finally, to confirm if the activation mechanism in $Co_{10}Ni_1$-MOF is the same as that of $Co_{15}Ni_1$-MOF, XPS spectra are obtained for $Co_{10}Ni_1$-MOF before and after activation and then compared with those of $Co_{15}Ni_1$-MOF (Figure S8). The XPS spectra of C 1s, O 1s and N 1s are analyzed in the same way as those of $Co_{15}Ni_1$-MOF described in the main paper.

First, upon comparing the peak positions of Mn-MOF with $Co_{10}Mn_1$-MOF before activation, the peak positions are highly consistent (Figures S9 and S10). This suggests that the presence of the two metals neither affects the bonds nor the oxidation states of the metals in the bimetallic MOF.

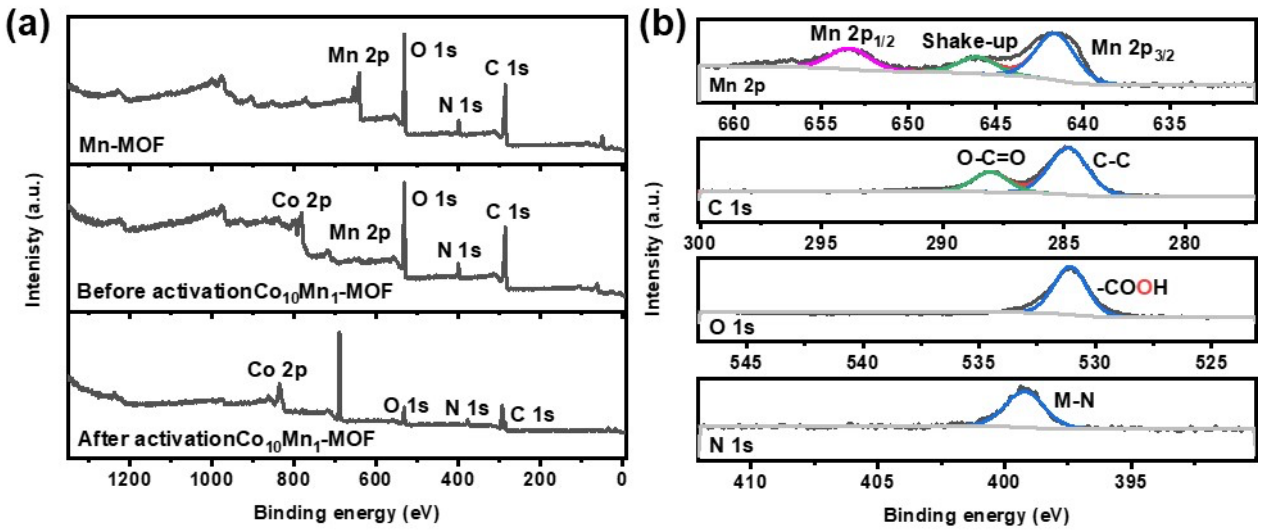


**Figure S9.** (a) Survey XPS spectra of Mn-MOF, before and after activation $Co_{10}Mn_1$-MOF and (b) high-resolution XPS spectra of Mn-MOF showing peaks corresponding to Mn 2p, C 1s, N 1s and O 1s.

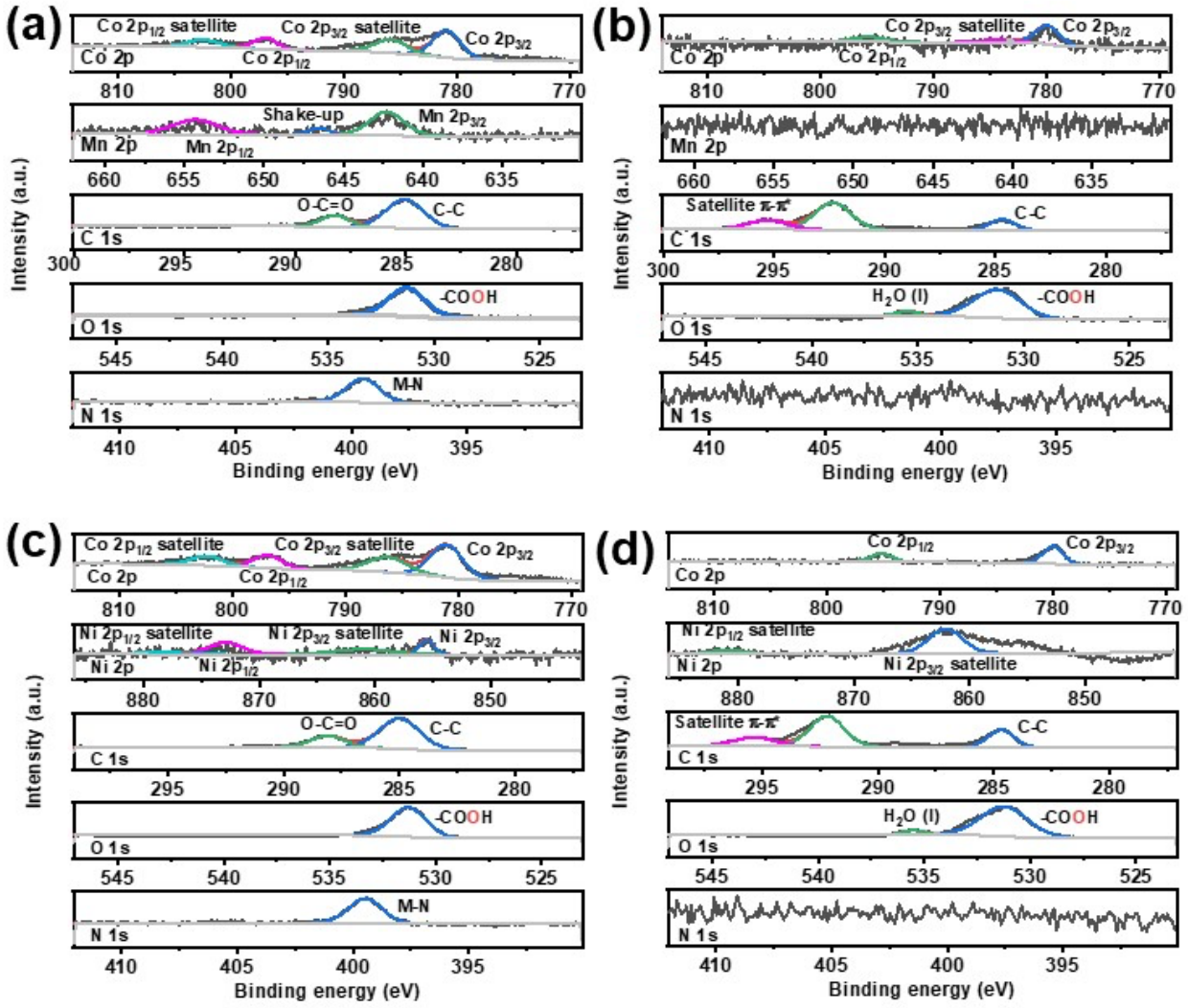


**Figure S10.** XPS spectra of $Co_{10}Mn_1$-MOF (a) before and (b) after activation. XPS spectra of $Co_{15}Ni_1$-MOF (c) before and (d) after activation.

As shown in Figures S10b and S10d, the XPS spectra of $Co_{10}Ni_1$-MOF after activation show no detectable peak associated with N 1s, just like $Co_{15}Ni_1$-MOF did. This also indicates that the surface metals in $Co_{10}Ni_1$-MOF are also converted to catalytically active)metal oxides/hydroxides. The oxidation state of Co in $Co_{10}Ni_1$-MOF before activation (Figure S10b) is found to be $Co^{2+}$, as only $Co^{2+}$ has prominent satellite peaks.